ACS APPLIED MATERIALS & INTERFACES

Research Article

www.acsami.org

Reduced Graphene Oxide Wrapped FeS Nanocomposite for Lithium-Ion Battery Anode with Improved Performance

Ling Fei,[†] Qianglu Lin,[†] Bin Yuan,[†] Gen Chen,[†] Pu Xie,[‡] Yuling Li,[†] Yun Xu,[†] Shuguang Deng,[†] Sergei Smirnov,[§] and Hongmei Luo*[,†]

[†]Department of Chemical Engineering, New Mexico State University, Las Cruces, New Mexico 88003, United States

[‡]Department of Mechanical and Aerospace Engineering, New Mexico State University, Las Cruces, New Mexico 88003, United States

[§]Department of Chemistry and Biochemistry, New Mexico State University, Las Cruces, New Mexico 88003, United States

ABSTRACT: A new nanocomposite formulation of the FeS-based anode for lithium-ion batteries is proposed, where FeS nanoparticles wrapped in reduced graphene oxide (RGO) are produced via a facile direct-precipitation approach. The resulting nanocomposite FeS@RGO structure has better lithium ion storage properties, exceeding those of FeS prepared without RGO sheets. The enhanced electrochemical performance is attributed to the robust sheet-wrapped structure with smaller FeS nanoparticles and synergetic effects between FeS and RGO sheets, such as increased conductivity, shortened lithium ion diffusion path, and the effective prevention of polysulfide dissolution.

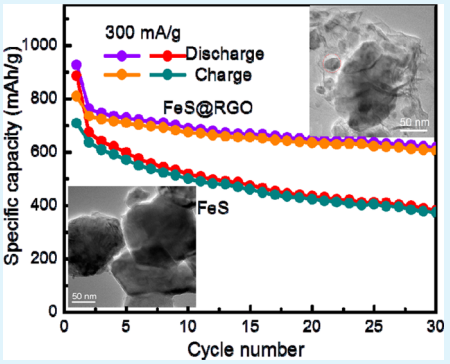

KEYWORDS: *FeS, reduced graphene oxide, nanocomposite, lithium-ion battery*

1. INTRODUCTION

The rapidly growing business of portable electronics (e.g., computers, mobile phones, cameras) has stimulated the rapid development of lithium-ion batteries (LIBs) due to their high energy density, flexible and lightweight design, and longer lifespan than conventional battery technologies. LIBs have also played a crucial role in hybrid electric vehicles (HEVs) and plug-in hybrid electric vehicles (PHEVs).[1,2] However, it should be pointed out that the performance of LIBs strongly depends upon the electrode materials. One major challenge in the development of LIBs is to find safe and cheap anode materials with large reversible capacity, desirable rate capability, long cycle life, and good compatibility with electrolyte and binder systems.[3,4] Graphite is the current commercially applied anode material, but it has a low theoretical capacity (372 mAh/g).[5,6] In the past decades, great effort has been devoted to studying transition-metal oxides for LIB anodes due to their higher capacity.[3,7−9] Recently, metal sulfides have also been considered as another promising class of materials with a high capacity.[10−24] Among them, iron sulfide, composed of inexpensive naturally abundant elements and having outstanding catalytic and electrochemical properties, has drawn particular research interest.[13,19,20]

However, iron sulfide suffers from large volume expansion during the insertion and extraction of Li ions.[19] More deleteriously, the lithium ion storage process in iron sulfide is accompanied with formation of insulating polysulfide Li_2S_x ($2 < x < 8$).[14,24] The polysulfide not only is soluble in organic electrolyte but also can gradually migrate to the cathode side, resulting in a severe loss of active materials and poor cyclic performance of the battery. In addition, polysulfide can form an insulating layer outside the electrode, which severely decreases the conductivity and even prevents further electrochemical reactions.[19,20] Reducing the particle size of FeS or coating them with a carbon layer have been proven effective in alleviating the dissolution problems.[19,25,26] For example, $Fe_{0.46}S$ embedded in carbon microspheres prepared via a solvothermal process exhibited excellent retention of capacity and high-rate performance;[19] carbon-coated FeS nanosheets via a surfactant-assisted solution method also showed a greater enhanced cycle performance and the specific capacities higher than those of FeS.[20] In addition to carbon coating, graphene and reduced graphene oxide (RGO) are also used as excellent hosts for loading active materials because of their unique two-dimensional structure, high specific surface area, excellent electronic conductivity, and chemical resistance.[2,27] In other words, graphene or RGO are able to increase the conductivity of nanocomposite materials and cushion the volume change stress experienced by active materials during charging and discharging. A large number of reports have demonstrated that introduction of graphene or RGO into either metal oxides or sulfides results in remarkably enhanced battery performance when compared to the corresponding pure metal oxides or sulfides.[8,12,28−31]

Received: April 5, 2013
Accepted: May 14, 2013
Published: May 14, 2013

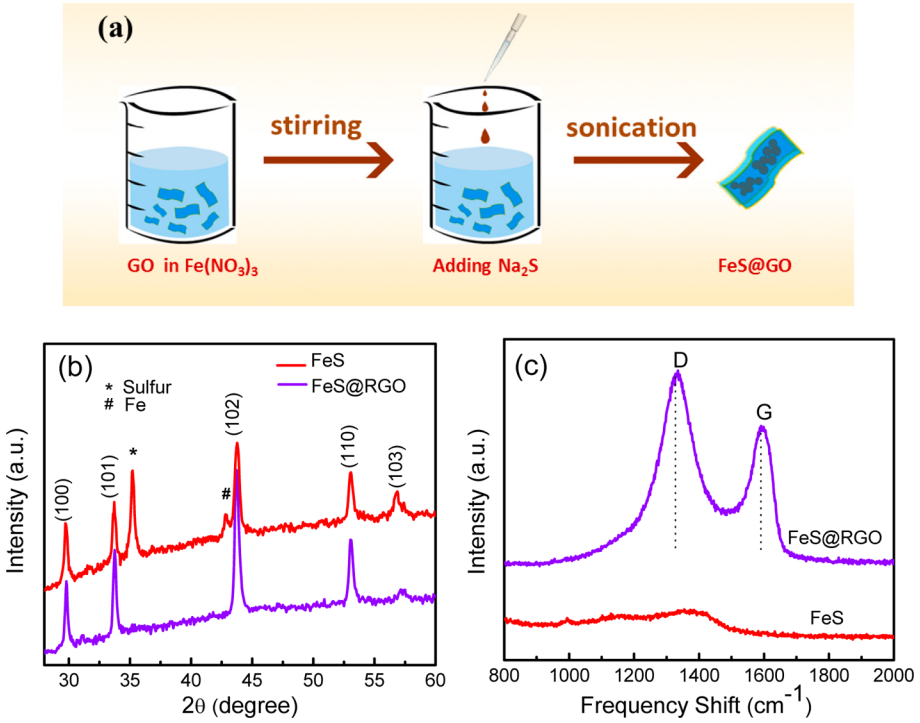

Figure 1. (a) Schematic illustration of the synthesis of FeS@GO composite. (b) XRD patterns of FeS and FeS@RGO nanocomposite. (c) Raman spectra of FeS and FeS@RGO nanocomposite.

Herein, we report on the preparation of FeS@RGO nanocomposite via a facile direct-precipitation route, followed by a postannealing method, and compare its performance with the sample prepared without RGO. It was found that the wrapping layer of RGO sheets not only reduced FeS particle sizes but also enhanced its electrochemical performance for LIBs anodes.

2. EXPERIMENTAL SECTION

2.1. Preparation of FeS and FeS@RGO Nanocomposite. Graphene oxide (GO) was synthesized from natural graphite by a modified Hummers method.[32] In a typical synthesis of the FeS@RGO composite, 2.02 g of $Fe(NO_3)_3{\cdot}9H_2O$ was dissolved in 20 mL of deionized (DI) water, and 6 mL of GO suspension (~5 mg/mL) was added to the solution under vigorous stirring. The mixture was sonicated for 1 h, followed by dropwise adding fresh $Na_2S{\cdot}9H_2O$ solution (1.802 g in 10 mL of DI water) under vigorous stirring. A black precipitate was formed immediately. The mixture was under continuous stirring for 1 h and sonicated for another 1 h. The precipitate was collected by vacuum filtration and washed six times with DI water. Finally, the precipitate was transferred to a quartz tube furnace and annealed at 400 °C in an argon atmosphere for 2 h to reduce GO and increase the crystallinity of FeS. FeS was prepared under the same conditions, but without adding the GO suspension.

2.2. Characterization. The structure, composition, and morphology of the samples were characterized by X-ray diffraction (XRD, Cu Kα), transmission electron microscopy (TEM; JEOL-2010, 200 kV), and scanning electron microscopy (SEM, S-3400NII) equipped with energy-dispersive X-ray spectrometry (EDS). Raman spectra were collected using a Renishaw Raman microscope with 632.8 nm (1.96 eV) laser excitation. Electrochemical measurements were conducted using CR-2032 coin cells. The working electrode was prepared by casting slurry (70 wt % of active materials, 20 wt % of carbon black, and 10 wt % of polyvinylidene fluoride binder in *N*-methyl-2-pyrrolidinone) onto nickel foam and dried in a vacuum oven at 70 °C for 12 h to remove the solvent. A lithium foil was used as the counter electrode, and a mixture of 1 M $LiPF_6$ in ethylene carbonate (EC)/dimethyl carbonate (DMC) (1:1 in volume) was used as the electrolyte. Cell assembly was carried out in an argon-filled glovebox with an oxygen concentration below 1 ppm. The galvanostatic charge/discharge measurements were performed using a Land battery testing system in the cutoff voltage window of 0.005−3 V (vs Li^+/Li). The cyclic voltammetry (CV) and the electrochemical impedance were measured using a Princeton Applied Research Versa STAT4 electrochemical workstation and a CHI-680A (CH Instruments, Inc.) workstation, respectively.

3. RESULTS AND DISCUSSION

The procedure for the preparation of the FeS@GO nanocomposite is illustrated in Figure 1a. The GO suspension was first dispersed in $Fe(NO_3)_3$ solution. Under ultrasonication, Fe^{3+} ions were adsorbed on the GO surface due to the functional groups (e.g., −OH, −COOH) and defects on the GO surface.[8,33] Introduction of Na_2S leads to the formation of the FeS precipitate as the following reaction is taking place

$$2Fe(NO_3)_{3(aq)} + 3Na_2S_{(aq)} \rightarrow 6NaNO_{3(aq)} + S_{(s)} + 2FeS_{(s)}$$

The stirring and utrasonicating ensure that the resulting precipitates are wrapped within GO sheets. In the subsequent postannealing step in argon, FeS was crystallized. We consider that, after this step, GO was partially reduced to RGO. According to ref 34, annealing GO in argon at temperatures below 600 °C can vaporize free and intercalated H_2O, remove carboxylic groups (but not −OH), and exfoliate GO. It is worth clarifying that the reason for using Fe^{3+} as a precursor instead of Fe^{2+} is to generate extra sulfur to compensate its loss in the annealing step. The XRD patterns of FeS and FeS@RGO are shown in Figure 1b. All the diffraction peaks of the FeS@RGO nanocomposite can be exclusively attributed to FeS (JCPDS 65-9124). In contrast, the XRD pattern of the FeS sample

dx.doi.org/10.1021/am401239f | ACS Appl. Mater. Interfaces 2013, 5, 5330−5335

shows an additional (201) peak from S (JCPDS 52-1035) and a (100) peak from Fe (JCPDS 50-1275). (The FeS sample is not pure, but it is main phase. Here, we still use FeS to note it for convenience.) No iron oxide impurites were detected. The result that only FeS was observed in the composite sample may suggest that RGO sheets help in preventing decomposition of FeS to Fe in the annealing process. The Raman spectra of both FeS and the FeS@RGO nanocomposite are shown in Figure 1c. For the composite, the two sharp peaks located at 1334 and 1589 cm^{-1} are the characteristic peaks of carbon material: the disorder-induced D band and the graphitic G band.[35] The high intensity ratio of the D and G bands (I_D/I_G = 1.3) indicates that there are plenty of defects on the surface of RGO, beneficial for adhesion of FeS nanoparticles to RGO nanosheets.

SEM images in Figure 2a,b show the morphology of as-prepared products over a large area. The FeS crystals are more

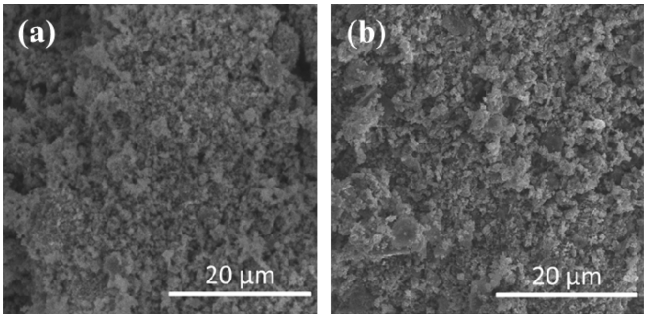

Figure 2. SEM images of FeS (a) and FeS@RGO nanocomposite (b).

uniformly distributed than the FeS@RGO nanocomposite where clusterization is more pronounced. These clusters are apparently due to the aggregation induced by RGO sheets. The RGO amount is roughly 12 wt % from EDS analysis (not shown here). TEM images shown in Figure 3 illustrate that RGO sheets do not just form conformal layers on individual FeS nanoparticles but rather trap multiple nanoparticles as peas in a pod. The FeS nanoparticles prepared without GO, shown in Figure 3a, have an average diameter of ca. 150 nm, whereas in the composite (Figure 3b), their size distribution is broader and a majority of them are smaller than in the FeS sample. For example, the circled FeS nanoparticle in the composite shown in Figure 3c has a diameter of ~28 nm. This suggests that the inclusion of GO sheets in the precursor restricts aggregation of newly formed FeS nanoparticles during the precipitation and coalescence in the postannealing process. The high-resolution TEM image of a single particle (Figure 3d) also shows that the crystallized nanoparticles are surrounded by crinkled RGO sheets.

The RGO-wrapped FeS composite makes it promising for application as an LIB anode material. Thus, prepared materials were assembled into half-cells and evaluated by galvanic charge and discharge in a voltage range of 0.005−3 V (vs Li^+/Li). Figure 4a presents the discharge/charge voltage profile of FeS@RGO for the 1st, 2nd, and 15th cycles at a current density of 100 mA/g. The nanocomposite delivered an initial discharge capacity of 1357 mAh/g and a charge capacity of 1116 mAh/g, giving an irreversible capacity loss of 18% and a low Coulombic efficiency of 82%. The initial irreversible lithium consumption and the inevitable formation of a solid electrolyte interface (SEI) layer are responsible for the large first-cycle loss and low Coulombic efficiency.[20] In the subsequent discharge cycle, a

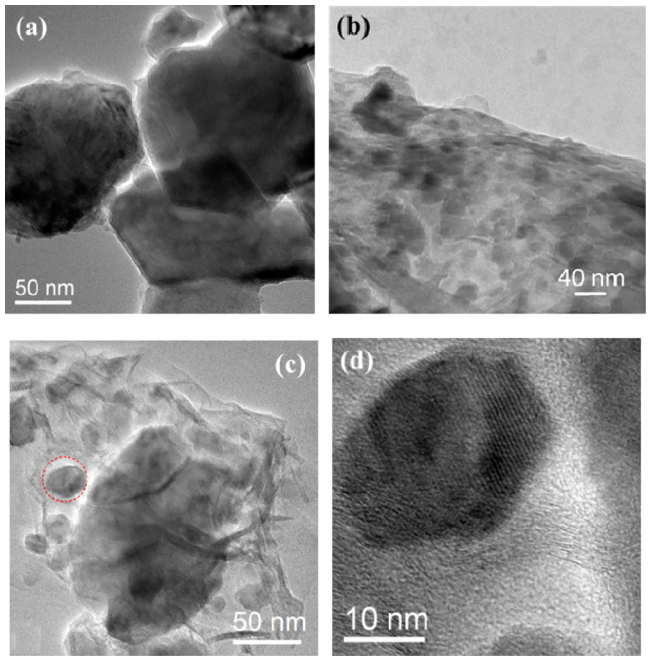

Figure 3. TEM images of (a) FeS and (b) FeS@RGO composite. (c) High-resolution image of FeS@RGO composite; the one circled in red is an example of the wrapped FeS nanoparticles. (d) HRTEM of the FeS nanoparticle within RGO.

capacity of 1142 mAh/g was delivered, remaining 84% of the first-cycle discharge capacity (1357 mAh/g). The second cycle delivers a charge capacity of 1076 mAh/g with the Coulombic efficiency rising up to 94%. After the 15th cycle, it still delivers a specific discharge capacity of 1064 mAh/g and a charge capacity of 1039 mAh/g with the Coulombic efficiency achieving 97.6%. Additionally, the first discharge cycle has a large plateau at around 1.3 V, whereas the plateau in the subsequent discharge cycles is observed at 1.5 V. The plateau position is the same as that in the previous study conducted by Goodenough et.al.[14] In another work, both the first and the second discharge profiles show a plateau around 1.4 V.[20] Factors such as different structure and preparation method may possibly shift the plateau position in a small range. The cycle performance of FeS@RGO at a current density of 100 mA/g is displayed in Figure 4b. The composite shows a very stable cyclic performance with its capacity remaining as high as 978 mAh/g even after 40 cycles. This value is almost 3 times the capacity of a commercial graphite anode (372 mAh/g), and is comparable to those reported in the literature.[13,19,20] The rate performance of FeS@RGO evaluated at different current densities is displayed in Figure 4c. As expected, the specific capacity decreased with increasing the current density: the electrode delivered a capacity of ~660 mAh/g at 200 mA/g, 530 mAh/g at 300 mA/g, 400 mAh/g at 500 mA/g, and 200 mAh/g at 1000 mA/g, respectively. When the current density was changed back to 200 mA/g, the specific capacity rebounded to 510 mAh/g, which is still higher than the theoretical capacity of graphite. Figure 4d compares the cycle performance of FeS and FeS@RGO at the same current density of 300 mA/g. In the 1st, 10th, and 30th discharge cycles, the composite delivered a discharge capacity of 927, 690, and 618 mAh/g, respectively, whereas FeS suffered a rapid decline of the capacity with 885, 518, and 382 mAh/g, respectively. The TEM image of FeS@RGO after 40 discharge−charge cycles at a

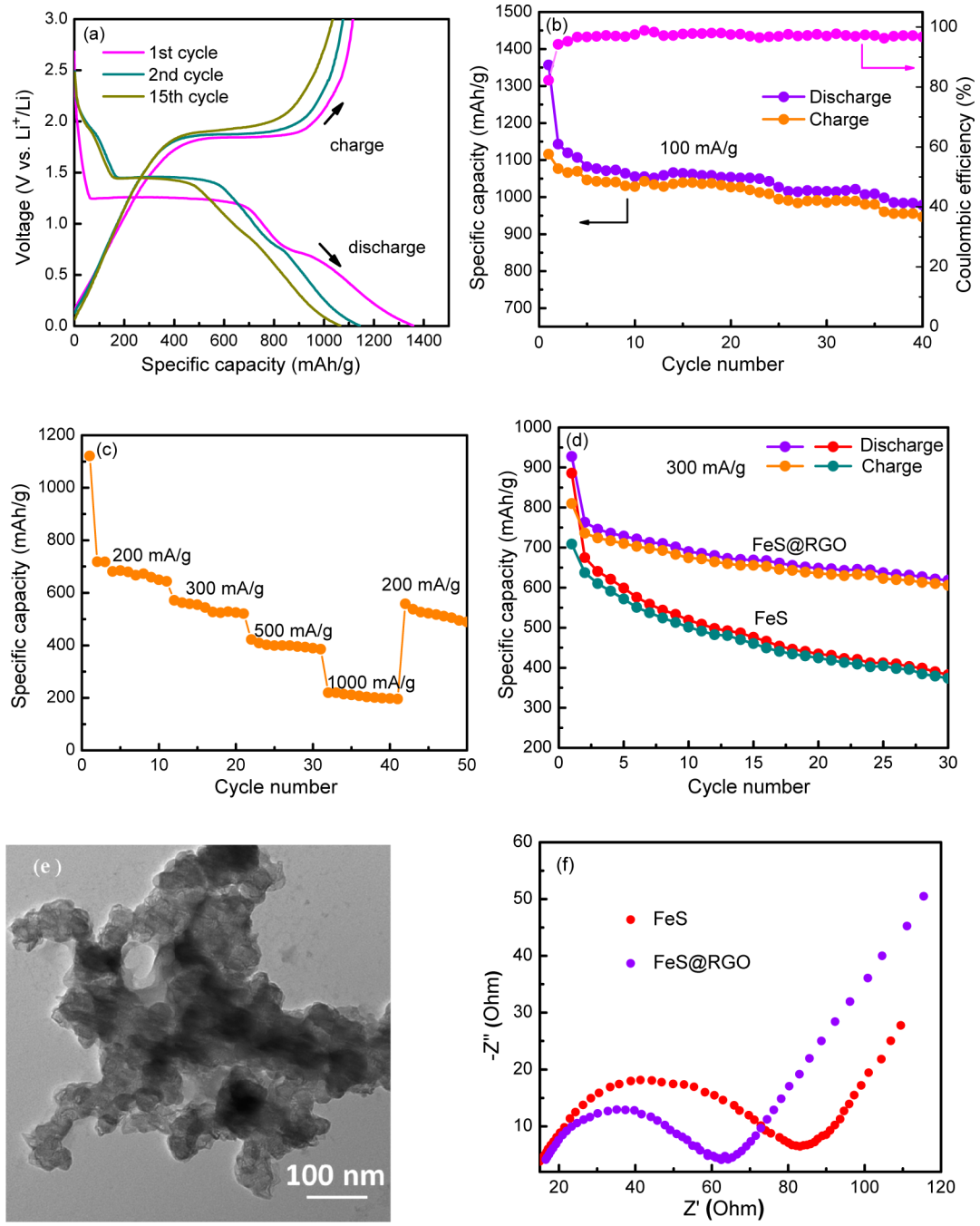

Figure 4. (a) Voltage profile of FeS@RGO at 100 mA/g. (b) Cycle performance of FeS@RGO nanocomposite at a current density of 100 mA/g. (c) Rate performance of the FeS@RGO nanocomposite. (d) Cycle performance of FeS and FeS@RGO nanocomposite at a current density of 300 mA/g. (e) TEM image of FeS@RGO after 40 discharge−charge cycles at a current density of 100 mAh/g. (f) Nyquist plots for FeS and FeS@RGO nanocomposite at zero bias.

current density of 100 mA/g was taken to study the structure stability. As shown in Figure 4e, the material still remains as a whole body. No fragments or pulverized individual particles were observed, which further confirms that the wrapping structure is very robust. Electrochemical impedance of FeS and FeS@RGO was also measured to understand their interfacial properties. As seen in Figure 4f, the Nyquist plots for both electrodes consist of a semicircle with the charge-transfer resistance at the electrode interface, while the straight line (Warburg line) in the low-frequency region is attributed to ion diffusion in the electrolyte to the electrode interface. The smaller semicircle for FeS@RGO indicates a lower electrochemical resistance than that of FeS.[19] This result again confirms that the interconnected RGO thin layers can increase the electrochemical conductivity of overall electrodes.

The improved electrochemical performance of FeS@RGO can be attributed to the unique nanocomposite architecture of FeS particles wrapped inside RGO sheets. The contact area between the FeS nanoparticles and the RGO is enhanced due to the flexible nature of thin layered RGO nanosheets. This thin carbon layer not only increases the electrode conductivity but also acts as a buffer layer that maintains the structural integrity

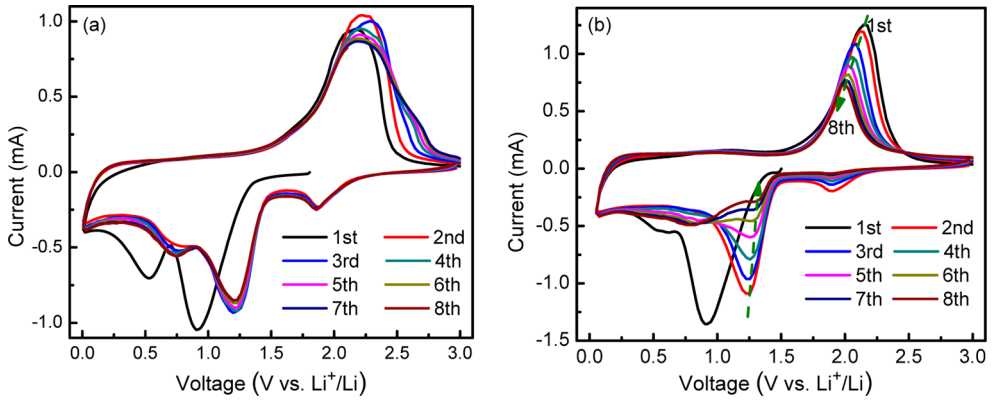

Figure 5. Cyclic voltammetry profiles of the first eight cycles for (a) FeS@RGO and (b) FeS.

of the electrode despite large volume changes during the charging and discharging cycles, as well as hinders aggregation of FeS particles. Most importantly, the RGO wrapping layer reduces the dissolution of polysulfide by absorbing and trapping it inside.[20,36,37] Additionally, the reduced particle size of FeS as compared with bare FeS may effectively shorten the diffusion pathway for Li ions and increase the effective area, both contributing to a faster charge transfer. Therefore, the nanocomposite exhibits a significantly enhanced electrochemical performance and is more suitable for LIB applications.

To better understand the redox reactions taking place in the electrodes, a cyclic voltammetry (CV) study was performed. The first eight cycles for both FeS and FeS@RGO were recorded at the scan rate of 0.5 mV/s in the voltage window of 0.005−3 V vs Li^+/Li. As shown in Figure 5, a large reduction peak at ca. 0.9 V in the initial cycle was observed for both electrodes, and it corresponds to the reaction[20]

$$FeS + 2Li^+ + 2e^- \rightarrow Li_2S + Fe$$

The peak around 0.5 V is attributed to the formation of the SEI layer on the surface of the active material. The oxidation peak around 2 V in the first cycle is caused by oxidation of Fe to $Li_{2-x}FeS_2$.[13,20] The shape of CV changes after the first cycle, indicating that the reactions are different in the subsequent cycles.[38] In the second and subsequent lithiation cycles, two reduction peaks appearing around 1.85 and 1.25 V are related to the step-by-step formation of Li_2FeS_2 from the $Li_{2-x}FeS_2$ phase.[38,39] The peak around 2 V appearing after the first cycle is related to the delithiation process (Li_2FeS_2 to $Li_{2-x}FeS_2$).[20] The reaction between $Li_{2-x}FeS_2$ and Li_2FeS_2 is reversible, which makes FeS applicable for LIB electrode material. Noticeably, FeS exhibits an obvious decline of both anodic and cathodic peaks and a clear shift along the arrow direction. The FeS@RGO composite, on the other hand, shows minimal changes in the CV curves after the first cycle; all curves almost overlap, suggesting excellent reversibility of the electrode and better structural stability.

4. CONCLUSION

In summary, we have demonstrated a facile direct-precipitation route for preparing FeS and the FeS@RGO nanocomposite. Wrapping of FeS nanoparticles in RGO sheets has been proven to have a profound influence on the properties of FeS, such as decreasing the particle size, increasing electrode conductivity, maintaining structural integrity, and minimizing the negative effect of polysulfides. The FeS@RGO demonstrates excellent Li ion storage properties with high specific capacities and stable charge/discharge performance. Moreover, the direct-precipitation route is a very simple and cost-effective method that can be easily scaled up. This further makes the FeS@RGO nanocomposite a promising anode material for lithium-ion batteries.

AUTHOR INFORMATION

Corresponding Author

*Tel: 575-646-4204. Fax: 575-646-7706. E-mail: hluo@nmsu.edu.

Notes

The authors declare no competing financial interest.

ACKNOWLEDGMENTS

We thank Dr. Peter Cooke for helping with SEM and acknowledge the funding support from the NSF under Grant No. 1131290. L.F. acknowledges the Preparing Future Faculty Award from the Graduate School at NMSU.

REFERENCES

(1) Lou, X. W.; Deng, D.; Lee, J. Y.; Feng, J.; Archer, L. A. *Adv. Mater.* **2008**, *20*, 258.
(2) Xu, Y.; Yi, R.; Yuan, B.; Wu, X.; Dunwell, M.; Lin, Q.; Fei, L.; Deng, S.; Andersen, P.; Wang, D.; Luo, H. *J. Phys. Chem. Lett.* **2012**, *3*, 309.
(3) Yan, N.; Hu, L.; Li, Y.; Wang, Y.; Zhong, H.; Hu, X.; Kong, X.; Chen, Q. *J. Phys. Chem. C* **2012**, *116*, 7227.
(4) Kim, M. G.; Cho, J. *Adv. Funct. Mater.* **2009**, *19*, 1497.
(5) Nam, S.; Kim, S.; Wi, S.; Choi, H.; Byun, S.; Choi, S.; Yoo, S.; Lee, K. T.; Park, B. *J. Power Sources* **2012**, *211*, 154.
(6) Wu, P.; Du, N.; Zhang, H.; Yu, J.; Qi, Y.; Yang, D. *Nanoscale* **2011**, *3*, 746.
(7) Zhang, B.; Zheng, Q. B.; Huang, Z. D.; Oh, S. W.; Kim, J. K. *Carbon* **2011**, *49*, 4524.
(8) Wu, Z. S.; Ren, W. C.; Wen, L.; Gao, L. B.; Zhao, J. P.; Chen, Z. P.; Zhou, G. M.; Li, F.; Cheng, H. M. *ACS Nano* **2010**, *4*, 3187.
(9) Fei, L.; Lin, Q.; Yuan, B.; Naeemi, M.; Xu, Y.; Li, Y.; Deng, S.; Luo, H. *Mater. Lett.* **2013**, *98*, 59.
(10) Vaughn, D. D.; Hentz, O. D.; Chen, S.; Wang, D.; Schaak, R. E. *Chem. Commun.* **2012**, *48*, 5608.
(11) Aso, K.; Sakuda, A.; Hayashi, A.; Tatsumisago, M. *ACS Appl. Mater. Interfaces* **2013**, *5*, 686.
(12) Gu, Y.; Xu, Y.; Wang, Y. *ACS Appl. Mater. Interfaces* **2013**, *5*, 801.
(13) Kim, B.; Takada, K.; Ohta, N.; Seino, Y.; Zhang, L.; Wada, H.; Sasaki, T. *Solid State Ionics* **2005**, *176*, 2383.
(14) Kim, Y.; Goodenough, J. B. *J. Phys. Chem. C* **2008**, *112*, 15060.
(15) Lai, C. H.; Lu, M. Y.; Chen, L. J. *J. Mater. Chem.* **2012**, *22*, 19.

(16) Liu, H.; Su, D.; Wang, G.; Qiao, S. Z. *J. Mater. Chem.* **2012**, *22*, 17437.
(17) Liu, Y.; Qiao, Y.; Zhang, W. X.; Li, Z.; Hu, X. L.; Yuan, L. X.; Huang, Y.-H. *J. Mater. Chem.* **2012**, *22*, 24026.
(18) Wang, Y.; Wu, J.; Tang, Y.; Lü, X.; Yang, C.; Qin, M.; Huang, F.; Li, X.; Zhang, X. *ACS Appl. Mater. Interfaces* **2012**, *4*, 4246.
(19) Wu, B.; Song, H.; Zhou, J.; Chen, X. *Chem. Commun.* **2011**, *47*, 8653.
(20) Xu, C.; Zeng, Y.; Rui, X.; Xiao, N.; Zhu, J.; Zhang, W.; Chen, J.; Liu, W.; Tan, H.; Hng, H. H.; Yan, Q. *ACS Nano* **2012**, *6*, 4713.
(21) Zhang, C.; Wang, Z.; Guo, Z.; Lou, X. W. *ACS Appl. Mater. Interfaces* **2012**, *4*, 3765.
(22) Pan, Q.; Xie, J.; Liu, S.; Cao, G.; Zhu, T.; Zhao, X. *RSC Adv.* **2013**, *3*, 3899.
(23) Zhong, H.; Yang, G.; Song, H.; Liao, Q.; Cui, H.; Shen, P.; Wang, C.-X. *J. Phys. Chem. C* **2012**, *116*, 9319.
(24) Chung, J. S.; Sohn, H. J. *J. Power Sources* **2002**, *108*, 226.
(25) Demir Cakan, R.; Titirici, M. M.; Antonietti, M.; Cui, G.; Maier, J.; Hu, Y. S. *Chem.Commun.* **2008**, 3759.
(26) Zhou, J.; Song, H.; Chen, X.; Zhi, L.; Yang, S.; Huo, J.; Yang, W. *Chem. Mater.* **2009**, *21*, 2935.
(27) He, Y. S.; Gao, P. f.; Chen, J.; Yang, X. w.; Liao, X. Z.; Yang, J.; Ma, Z. F. *RSC Adv.* **2011**, *1*, 958.
(28) Huang, Y.; Huang, X. L.; Lian, J. S.; Xu, D.; Wang, L. M.; Zhang, X. B. *J. Mater. Chem.* **2012**, *22*, 2844.
(29) Hsieh, C. T.; Lin, J. S.; Chen, Y. F.; Teng, H. *J. Phys. Chem. C* **2012**, *116*, 15251.
(30) Xu, C.; Sun, J.; Gao, L. *Nanoscale* **2012**, *4*, 5425.
(31) Chang, K.; Chen, W. *ACS Nano* **2011**, *5*, 4720.
(32) Hummers, W. S.; Offeman, R. E. *J. Am. Chem. Soc.* **1958**, *80*, 1339.
(33) Dreyer, D. R.; Park, S.; Bielawski, C. W.; Ruoff, R. S. *Chem. Soc. Rev.* **2010**, *39*, 228.
(34) Huh, S. H. Thermal Reduction of Graphene Oxide. In *Physics and Applications of Graphene-Experiments*; Mikhailov, S., Ed.; InTech: Rijeka, Croatia, 2011; Chapter 5.
(35) Evanoff, K.; Magasinski, A.; Yang, J.; Yushin, G. *Adv. Energy Mater.* **2011**, *1*, 495.
(36) Ji, X.; Lee, K. T.; Nazar, L. F. *Nat. Mater.* **2009**, *8*, 500.
(37) Yang, Y.; Yu, G.; Cha, J. J.; Wu, H.; Vosgueritchian, M.; Yao, Y.; Bao, Z.; Cui, Y. *ACS Nano* **2011**, *5*, 9187.
(38) Zhang, D.; Tu, J. P.; Xiang, J. Y.; Qiao, Y. Q.; Xia, X. H.; Wang, X. L.; Gu, C. D. *Electrochim. Acta* **2011**, *56*, 9980.
(39) Fong, R.; Dahn, J. R.; Jones, C. H. W. *J. Electrochem. Soc.* **1989**, *136*, 3206.